J Mater Sci: Mater Electron (2016) 27:12365–12373
DOI 10.1007/s10854-016-5024-1

Influence of RF power on structural optical and electrical properties of hydrogenated nano-crystalline silicon (*nc*-Si:H) thin films deposited by PE-CVD

Ashok Jadhavar[1] · Amit Pawbake[1] · Ravindra Waykar[1] · Vaishali Waman[1] · Sachin Rondiya[1] · Omkar Shinde[1] · Rupali Kulkarni[1] · Avinash Rokade[1] · Ajinkya Bhorde[1] · Adinath Funde[1] · Dinkar Patil[2] · Habib Pathan[3] · Sandesh Jadkar[3]

Received: 1 January 2016 / Accepted: 18 May 2016 / Published online: 24 May 2016
© Springer Science+Business Media New York 2016

Abstract We report synthesis of hydrogenated nanocrystalline silicon (*nc*-Si:H) thin films by using conventional plasma enhanced chemical vapor deposition (PE-CVD) system from gas mixture of pure silane (SiH_4) and hydrogen (H_2). We investigated the effect of RF power on structural, optical and electrical properties using various characterization techniques including Raman spectroscopy, FTIR spectroscopy, UV–visible spectroscopy etc. Low angle XRD and Raman spectroscopy analysis revealed that the RF power in PE-CVD is a critical process parameter to induce nanocrystallization in Si:H films. The FTIR spectroscopy analysis results indicate that with increase in RF power the predominant hydrogen bonding in films shifts from Si–H to Si–H_2 and (Si–H_2)$_n$ bonded species bonded species. However, the bonded hydrogen content didn't show particular trend with change in RF power. The UV–visible spectroscopy analysis shows that the band tail width (E_{04}–E_{Tauc}) with increase in RF power. The defect density and Urbach energy also increases with increase in RF power. The highest dark conductivity (and lowest charge carrier activation energy) was obtained for the film deposited at RF power of 125 W indicating that 125 W is optimized RF power of our PE-CVD unit. At this optimized RF power nc-Si:H films with crystallite size ~3.7 nm having good degree of crystallinity (~86.7 %) and high band gap (E_{Tauc} ~ 2.01 eV and E_{04} ~ 2.58 eV) were obtained with a low hydrogen content (6.2 at.%) at moderately high deposition rate (0.24 nm/s).

✉ Sandesh Jadkar
sandesh@physics.unipune.ac.in

[1] School of Energy Studies, Savitribai Phule Pune University, Pune 411 007, India

[2] Department of Metallurgical Engineering and Materials Science, IIT Powai, Mumbai 400 076, India

[3] Department of Physics, Savitribai Phule Pune University, Pune 411 007, India

1 Introduction

During a decade hydrogenated nanocrystalline silicon (*nc*-Si:H) thin films have attracted considerable attention due to its distinguishing characteristics, such as reduced photo-induced degradation, higher carrier mobility and conductivity, efficient visible photoluminescence, greater doping efficiency and [1–3] have been considered as a promising material to overcome the instability issues of a-Si:H devices for application in photovoltaic and opto-electronic devices [4]. This material holds great promise as a low-cost, high-efficiency photovoltaic thin film suitable for tandem cell applications [5].

Generally, there are two methods can be used for the preparation of crystalline silicon films (*nc*-Si, μc-Si and poly-Si), one is the re-crystallization of a-Si:H films and other is the direct deposition. The re-crystallization technique includes rapid thermal annealing [6], excimer laser crystallization [7], aluminium induced crystallization [8], etc. However, these methods have difficulties in accurate control of crystallite size and crystalline volume fraction. In addition, these methods usually undergoing post-annealing at high temperatures over 1000 °C which inevitably limits its further applications in opto-electronic devices. On the other hand, a variety of direct chemical vapor deposition (CVD) techniques has been used to yield materials with good optoelectronic properties. These include plasma enhanced CVD (PECVD) [9] and its variant, electron cyclotron resonance CVD [10], and hot wire CVD (HW-CVD) [11], magnetron sputtering [12], layer-

by-layer (LBL) deposition [9], very high frequency plasma-enhanced chemical vapor deposition (VHF-PE-CVD) [13] etc. Among these, only PECVD has been established for industrial applications in the solar cells industry and TFT technology.

It is generally believed that the properties of *nc*-Si:H thin films prepared by PE-CVD are strongly affected by the process parameters such as substrate temperature, process pressure, inter-electrode distance, RF power, hydrogen dilution of source gases etc. employed during the deposition. These studies are based on the understanding the influence of only one of these process parameters on *nc*-Si:H thin films. However, there is lot of room for the improvement of film properties since the relation between the variation of deposition parameter and the resulting film properties has not been fully elucidated yet. It is with this motivation that we initiated the detailed study of synthesis and characterization of un-doped *nc*-Si:H films using PE-CVD method. In this paper, we present the detail investigation of influence of RF power on structural, optical, and electrical properties of *nc*-Si:H films deposited by PE-CVD method. The obtained results exhibited that these properties critically depends on RF power.

2 Experimental

2.1 Film preparation

Intrinsic hydrogenated nanocrystalline silicon (*nc*-Si:H) thin films were deposited simultaneously on corning #7059 glass and c-Si wafers by locally fabricated plasma enhanced chemical vapor deposition (PE-CVD) unit. Figure 1 shows the schematic of locally fabricated PE-CVD employed for the deposition of nc-Si:H films. It consists of two stainless steel chambers, referred as process chamber and load lock chamber. The process chamber is coupled with a turbo molecular pump (TMP) and rotary pump which yields a base pressure less than 10^{-6} Torr. The use of load lock chamber prevents the process chamber to be directly exposed to air, which minimizes the pump down time and reduce contamination of layers with oxygen and water vapors. The substrates can be moved from load lock to process chamber by a pneumatically controlled transport arm using slit valve. The pressure during deposition was kept constant by using throttle valve. The reaction gases are introduced in the process chamber from specially designed gas shower to ensure uniform gas flow between two electrodes. The substrates can be placed on substrate holder which is heated by in build heater and substrate temperature varied by using in-build thermocouple and temperature controller. The RF power is feed through the upper electrode via matching network while substrate holder is grounded. The deposition parameters are listed in Table 1.

The glass substrates were cleaned with double distilled water whereas, the c-Si wafers were given an HF etch to remove native oxide layer. The substrates were loaded to the substrate holder and then the deposition chamber was evacuated to the base pressure less than 10^{-6} Torr. Prior to each deposition, the substrate holder and deposition chamber were baked for 2 h at 100 °C to remove any water vapor absorbed on the substrates and to reduce the oxygen contamination in the film. After that, the substrate temperature was brought to desired value by appropriately setting the inbuilt thermocouple and temperature controller. The deposition was carried out for desired amount of time and films were allowed to cool to room temperature in vacuum.

2.2 Film characterization

Low angle X-ray diffraction pattern were obtained by X-ray diffractometer (Bruker D8 Advance, Germany) using CuKα line ($\lambda = 1.54056$ Å). Dark conductivity (σ_{dark}) and photoconductivity (σ_{photo}) were measured using samples of dimension 3 cm × 1 cm deposited on glass substrate with coplanar Al electrodes 0.5 mm apart deposited by vacuum evaporation. The measurements were carried out at room temperature and atmospheric pressure. The activation energy (E_{act}) was calculated from,

$$\sigma = \sigma_0 \exp\left(-\frac{E_{act}}{kT}\right) \tag{1}$$

where k is the Boltzmann constant and T is the absolute temperature. The FTIR spectra were recorded in transmission mode by using FTIR spectrophotometer (JASCO, 6100-type A) in the range 400–4000 cm^{-1}. Bonded hydrogen content (C_H) was calculated from wagging mode of FTIR absorption peak using the method given by the Brodsky et al. [14]. The optical absorption coefficient (α) was determined from the transmission (% T) and reflection (% R) measurements using UV–visible spectrophotometer (JASCO, V-670). The band gap was estimated using the procedure followed by Tauc [15]. Raman spectra were recorded with Raman spectroscopy (Renishaw InVia Confocal Raman Microscope) in the wave number range 100–1000 cm^{-1}. The spectrometer has backscattering geometry for detection of Raman spectrum with the resolution of 1 cm^{-1}. The excitation source was 532 nm line of He–Ne laser. The power of the Raman laser was kept less than 10 mW to avoid laser induced crystallization on the films. For the calculation of crystalline fraction (X_{Raman}) and crystallite size (d_{Raman}) we have followed the method given by Kaneko et al. [16], and He et al. [17] respectively. Thickness of films was determined by profilometer (KLA

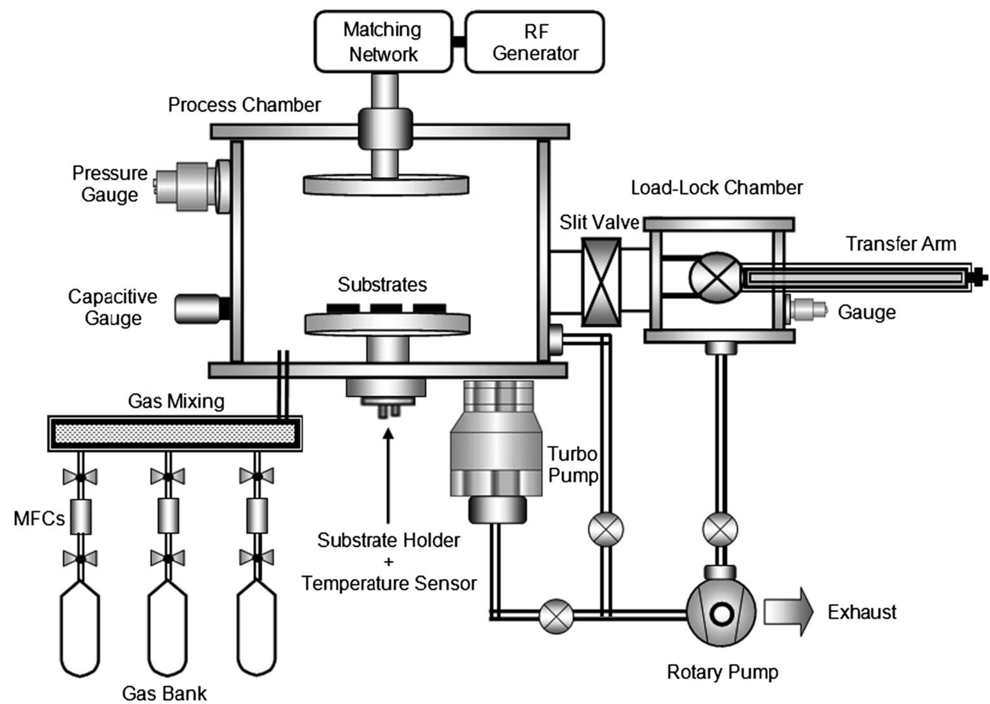

Fig. 1 Schematic of home-made PE-CVD employed for the deposition of *nc*-Si:H films in the present study

Table 1 Process parameters used of the deposition of intrinsic *nc*-Si:H thin films by PE-CVD method

Process parameter	Value
Deposition temperature (T_{Sub})	300 °C
Distance between electrodes	3 cm
Gas flow rates	
(1) Silane (F_{SiH_4})	1 sccm
(2) Hydrogen (F_{H_2})	70 sccm
Deposition pressure	300 mTorr
Deposition time	60 min

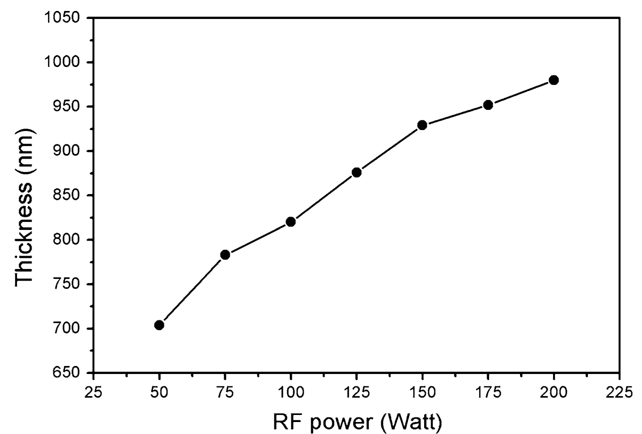

Fig. 2 Variation of thickness of Si:H films as a function of RF power

Tencor, P-16 +) and was further confirmed by UV–Visible spectroscopy using the method proposed by Swanepoel [18].

3 Results and discussion

3.1 Variation in thickness of film

Influence of RF power on thickness of Si:H films deposited using PE-CVD method is shown in Fig. 2. As seen from the figure the thickness of the films monotonically increases with increase in RF power. Generally, increase in RF power enhances the dissociation and ionization of SiH_4 gas molecules. It increases the flux of the depositing precursors to the substrate surface. As a result the thickness of the film increases with increase in RF power. This contributes to increase of the deposition rate.

3.2 Low angle XRD analysis

To identify the crystallinity and presence of material phase in the films deposited by PE-CVD at different RF powers, low angle x-ray diffraction (XRD) studies were carried out. The low angle XRD pattern of Si:H films deposited at different RF power are shown in Fig. 3. It is evident from the figure that films deposited at low RF power (50 and 75 W) show only a broad shoulder centered at $2\theta \sim 27°$ indicating that films are amorphous. Films deposited with increase in RF power (100, 125 and 150 W) the XRD

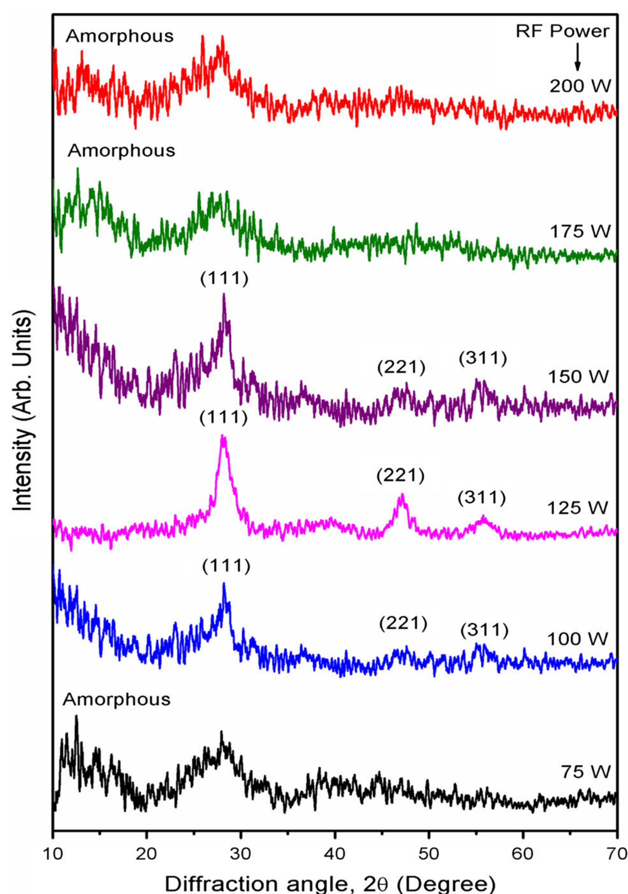

Fig. 3 Low angle XRD pattern of Si:H films deposited at different RF power using PE-CVD method

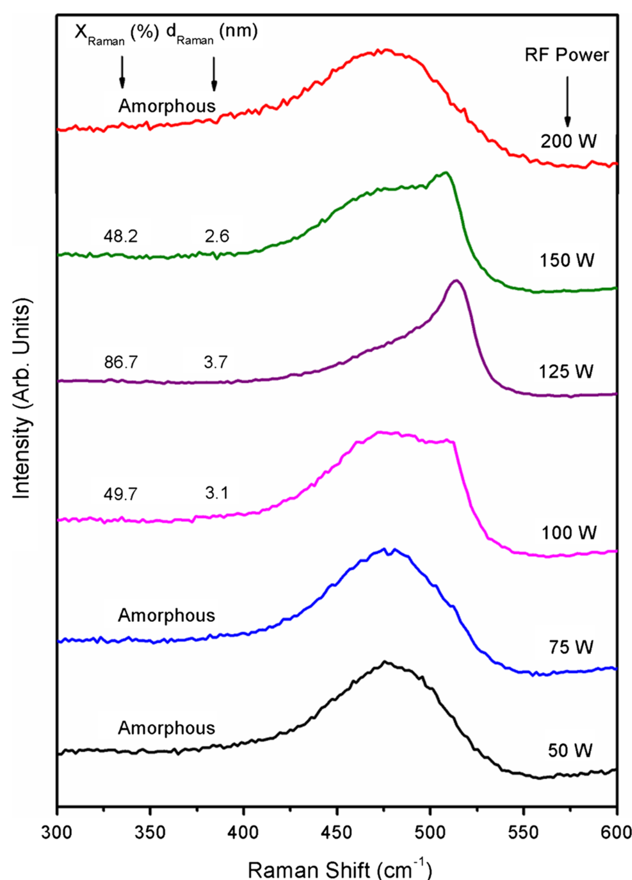

Fig. 4 Raman spectra of Si:H films deposited at different RF power using PE-CVD method

pattern show three peaks at 2θ ~ 28.4°, 47.5° and 56.1° corresponding to (111), (220) and (311) crystal orientations, respectively indicating that these films contain nanocrystalline-Si phase. The dominant peak is (111), indicating that the crystallites in the film have preferential orientation in (111) direction. However, the films deposited with further increasing RF power (175 and 200 W) the diffraction peaks corresponding to all the crystallographic planes were disappears and a broad hump around 2θ ~ 27° has been emerge without any evidence of crystallinity. These results are consistent with the Raman results (discussed later). Therefore, from low angle XRD analysis it is concluded that employment of moderate RF power in PE-CVD is essential for the growth of nanocrystalline Si:H films.

3.3 Raman spectroscopy analysis

Raman spectroscopy is a very powerful non-destructive technique used to investigate the structure of materials because it gives a fast and simple way to determine the phase of the material, whether it is amorphous, crystalline or nanocrystalline. Figure 4 shows the Raman spectra of the silicon films deposited at different RF power (P_{RF}) ranging from 50 to 200 W. To estimate the volume fraction of crystallites (X_{Raman}) and crystallite size (d_{Raman}), each spectrum in Fig. 4 was de-convoluted into three peaks (Two Gaussian peaks and one Lorentzian peak) with a quadratic base line using Levenberg–Marquardt method [19], a crystalline peak (~520 cm^{-1}), an amorphous peak (~480 cm^{-1}) and an intermediate peak (~510 cm^{-1}). Typical de-convoluted Raman spectra for Si:H film deposited at P_{RF} = 125 W is shown in Fig. 5. The crystalline fraction (X_{Raman}) was calculated from [16],

$$X_{Raman} = \frac{I_c + I_m}{I_c + I_m + I_a} \quad (2)$$

where I_c is the integrated intensity of the crystalline phase near 520 cm^{-1}, I_m is the integrated intensity of the intermediate phase around 500 cm^{-1} and I_a is the integrated intensity of the amorphous phase at 480 cm^{-1}. The crystallite size (d_{Raman}) was deduced using,

$$d_{Raman} = 2\pi\sqrt{\left(\frac{\beta}{\Delta\omega}\right)} \quad (3)$$

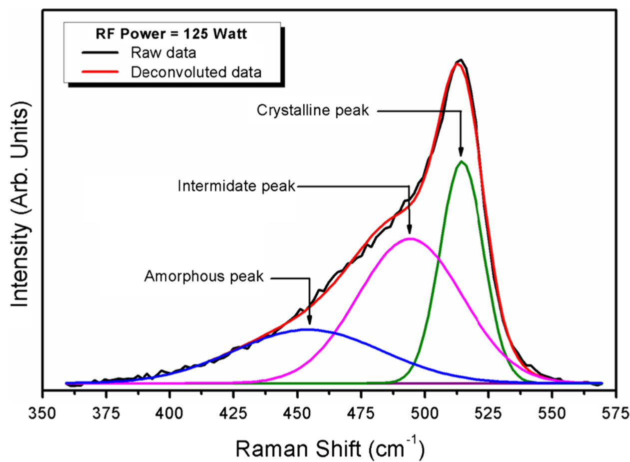

Fig. 5 Typical de-convoluted Raman spectra of Si:H films deposited at RF power 125 W using PE-CVD

Where $\Delta\omega$ is the peak shift compared to c-Si peak located $\sim$520 cm^{-1} and $\beta = 2.0$ cm^{-1}nm^2 [17].

As seen from Fig. 4 films deposited at low RF power (50 and 75 W) show only a broad shoulder centered $\sim$480 cm^{-1} which corresponds to typical a-Si:H material. However, the film deposited at RF power 100 W, shows the onset of nanocrystallization. The Raman spectra for this film show a broad shoulder centred $\sim$480 cm^{-1}, associated with the amorphous and the other Transverse Optic (TO) phonon peak centred $\sim$511 cm^{-1} originating from nanocrystalline phase [20]. For this film, X_{Raman} is $\sim$49.7 % and d_{Raman} is $\sim$3.1 nm. Further decrease in RF power, the peak shift towards higher wave number and its intensity enhances indicating increase in volume fraction of crystallites and its size. As a result, the film deposited at RF Power 125 W, the Raman spectra shows nanocrystalline phase with the TO phonon peak centred $\sim$515 cm^{-1} and a small amorphous content in it. For this film, X_{Raman} is $\sim$86.7 % and d_{Raman} is $\sim$3.7 nm. This clearly indicates that with increase in RF power in PE-CVD results in an amorphous-to-nanocrystalline transition in the film. However, further increase in RF power to 150 W the TO peak shift towards lower wave number and its intensity decline signifying decrease in volume fraction of crystallites and its size. For this film, X_{Raman} is $\sim$48.2 % and d_{Raman} is $\sim$2.6 nm. The Raman spectra for the film deposited at RF power 200 W the TO peak associated nanocrystalline phase disappear completely and a broad shoulder associated with the amorphous phase emerged at $\sim$480 cm^{-1} suggesting amorphization of the film. Tong et al. [21] had also reported similar results for *nc*-Si:H films deposited by using layer-by-layer (LbL) deposition technique. Increase in RF power directly increases the hydrogen etching effect and therefore induces the crystallization in the films

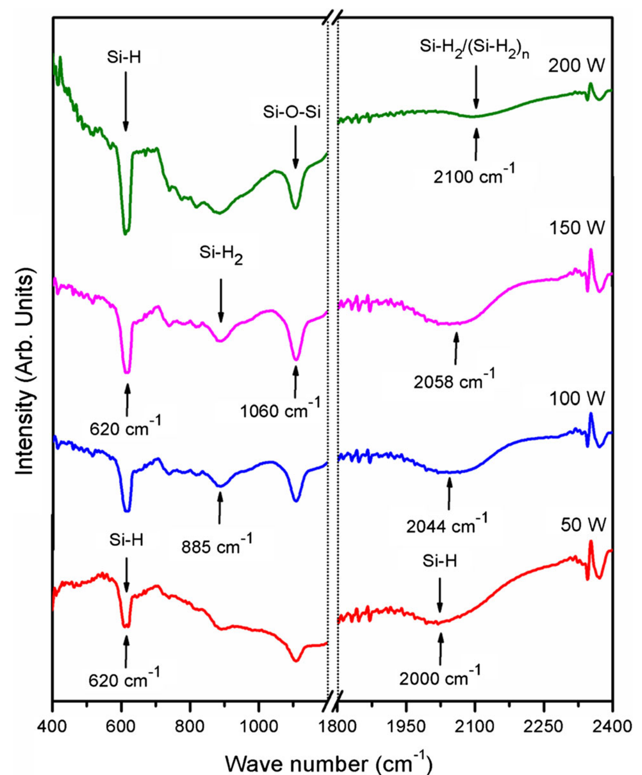

Fig. 6 FTIR spectra of *nc*-Si:H films (at normalized thickness) deposited by PE-CVD at different RF powers

deposited at 100, 125 and 150 W. However, further increase in RF power to 200 W causes the hydrogen etching effect to suppress the growth of crystallites. The high RF power increases the ion bombardment effect on the growth surface, which deteriorated the growth of crystallites on the growing surface and increases the structural disorder. These effects result in the reduction of crystallinity in the films. Therefore, from Raman spectroscopy analysis it is concluded that the RF power in PE-CVD is a critical process parameter to induce nanocrystallization in Si:H films.

3.4 Fourier transform infra red (FTIR) spectroscopy analysis

To study the hydrogen bonding configuration and to estimate the total hydrogen content in the film FTIR spectroscopy was used. The FTIR spectra of *nc*-Si:H films (at normalized thickness) deposited by PE-CVD method at different RF powers are shown in Fig. 6. For clarity, the spectra have been broken horizontally into two parts. It can be seen from the spectra that all films have two major absorption bands centered at $\sim$620 and $\sim$2000 cm^{-1} corresponding to the wagging/stretching modes, respectively, of vibrations of mono-hydrogen (Si–H) bonded

species [22]. The spectra also exhibits an absorption peak centered ~1095 cm^{-1} associated with the asymmetric Si–O–Si stretching vibrations. This is indicative of an oxidation effect caused by its porous-like microstructure, which is a typical feature for undoped nc-Si:H thin films [23]. In addition to these vibrational modes, an absorption peak centered ~885 cm^{-1} has been also observed with lesser intensity and assigned to the bending vibrational modes of $Si–H_2$ and $(Si–H_2)_n$ complexes [24]. With increase in RF power the intensity of absorption band at ~630 cm^{-1} increases. These results indicates that the hydrogen in the films predominantly incorporated in mono-hydrogen (Si–H) species. With increase in RF power the intensity of absorption band at ~620 cm^{-1} increases and at the same time intensity of absorption band centered at ~2000 cm^{-1} turn down and it shifts toward higher wave number 2100 cm^{-1}. The absorption band centered ~2100 cm^{-1} can be assigned to stretching vibrational modes of di-hydride, $Si–H_2$ and poly-hydride, $(Si–H_2)_n$ bonded species (isolated or coupled) respectively [25]. These results indicate that with increase in RF power the predominant hydrogen bonding in films shifts from Si–H to $Si–H_2$ and $(Si–H_2)_n$ bonded species bonded species. It was observed that the hydrogen content (C_H) in Si:H materials calculated from different methods is quite different. However, it has been reported that the integrated intensity of the peak at 620 cm^{-1} is the best measure of hydrogen content and other bands are less reliable [26]. Whatever may be the nature of the hydrogen bonding configuration; Si–H, $Si–H_2$, $(Si–H_2)_n$, $Si–H_3$ etc., all types of the vibration modes will contribute to the 620 cm^{-1} absorption band [27]. Thus, the hydrogen content has been estimated by using integrated intensity of the peak at 620 cm^{-1} by taking the oscillator strength value determined by Knights et al. [24]. Figure 7 shows the variation of hydrogen content (C_H) as a function of RF power. As seen from the figure, hydrogen

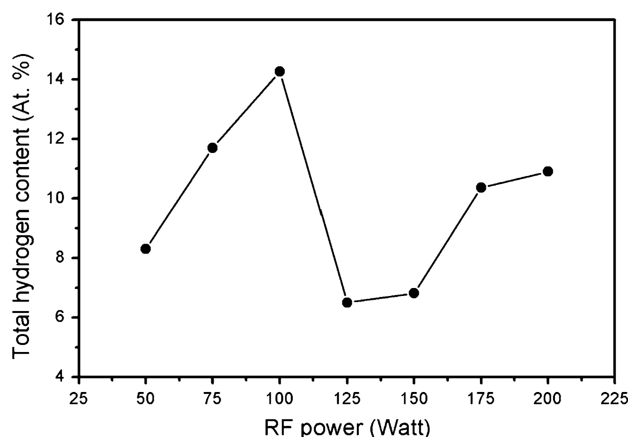

Fig. 7 Variation of hydrogen content as a function of RF power for Si:H films deposited by PE-CVD method

content first increases with increase in RF power from 50 to 100 W and then it decreases sharply with further increase in RF power up to 125 W. However, the hydrogen content increases gradually when RF power increased from 125 to 200 W. An increase in RF power increases the dissociation of SiH_4 and produces more SiH_x (x = 1, 2, 3) radicals [28]. The electron temperature also increases with increasing the RF power [29] which results in increasing the sticking probability of the deposition precursors. As a result, hydrogen rich precursors incorporated in the film and the hydrogen content increases. In addition, increase in RF power also increases the density of atomic H in the deposition chamber. The large number of atomic H reaching the growth surface enhances the surface diffusion of the growth precursors by covering more hydrogen on the growing surface [30]. It enhances the hydrogen etching effect [31] and amorphous-to-nanocrystalline transition occurs in the film and as a result hydrogen content increases with increase in RF power up to 125 W. Raman spectroscopy analysis support this conjecture. Increase in hydrogen content for the films deposited at RF power >125 W may attributed to the formation of defects or disorders or voids due to increase in ion bombardment effect on the growing surface and due to the amorphization of films as revealed from Raman spectroscopy analysis. The grain boundaries of defects and voids seem to be passivated by large amount of hydrides, silicon-hydrogen bonds suggesting increase of hydrogen content in the films at higher RF power.

3.5 UV–Visible spectroscopy analysis

Optical properties the films (band gap, refractive index, defect density and Urbach energy) were deduced from transmission (T) and reflection (R) spectra of the films deposited on corning glass using UV–visible spectrophotometer. In the direct transition semiconductor, the optical energy band gap (E_{Tauc}) and the optical absorption coefficient (α) are related by [15],

$$(\alpha E)^{1/2} = B^{1/2}(E - E_{Tauc}) \tag{4}$$

where α is the absorption coefficient, B is the optical density of state and E is the photon energy. The absorption coefficient (a) can be calculated from the transmittance of the films with the formula [32],

$$\alpha = \frac{1}{d}\ln\left(\frac{1}{T}\right) \tag{5}$$

where d is the thickness of the films and T is the transmittance. Therefore, the optical band gap is obtained by extrapolating the tangential line to the photon energy (E = hυ) axis in the plot of (αhυ) as a function of hυ.

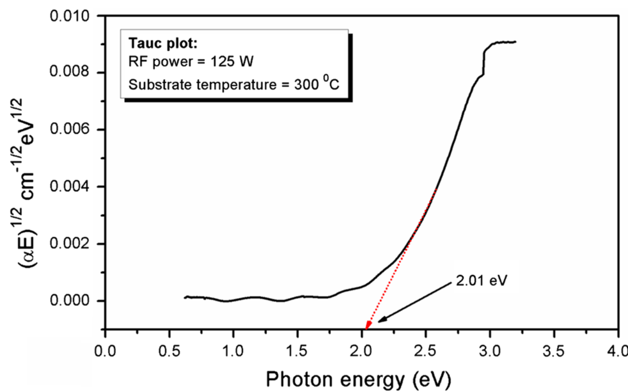

Fig. 8 Typical Tauc plot used to estimate optical band gap of Si:H film deposited at 125 W by PE-CVD method

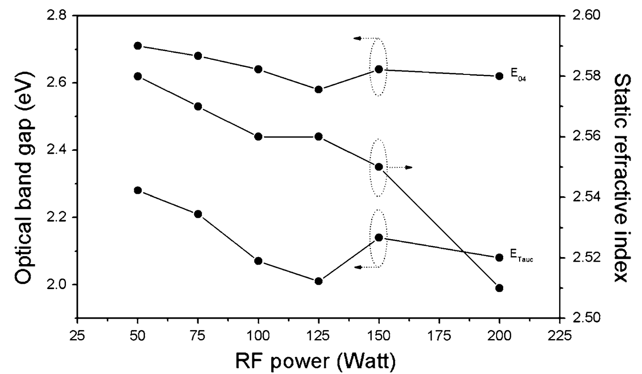

Fig. 9 Comparison of E_{Tauc} and E_{04} and variation of refractive index as a function of RF power for the films deposited by PE-CVD method

Typical optical band gap calculated using Tauc formula (E_{Tauc}) is shown in Fig. 8. It is agreed that the determination of band gap is not accurate using Tauc's formulation because of the extent of the valence and conduction band tails in the gap, especially in case of films where nanocrystallites are embedded in the amorphous matrix. However, it is expected to give an approximate estimate of the band gap. Thus, the energy where the absorption coefficient (α) is equal to 10^{-4} cm^{-1}, designated E_{04}, is also obtained from the transmission measurements. Figure 9 shows a comparison of E_{Tauc} and E_{04} as a function of RF power for the films deposited by PE-CVD method. It can be seen that E_{Tauc} decreases from 2.28 to 2.01 eV whereas E_{04} decreases from 2.71 to 2.62 eV when RF power increased from 50 to 200 W. As a result, band tail width of material taken as (E_{04}–E_{Tauc}) increases with increase in RF power. It is generally accepted that the band gap of Si:H depends on the hydrogen content and it linearly increases with the increase in hydrogen content in the films [33]. The band gap linearly increases from 1.5 to 1.7 eV when the hydrogen content in the film increases from 2 to 11 at.%. Then up to a hydrogen contents of 20 at.%, the band gap remains constant [34]. However, in the present study, no specific trend has been found between hydrogen content with RF power whereas band gaps, both, E_{Tauc} and E_{04} decreases with increase in RF power. Also, hydrogen content was found less than 14 at.% over the entire range of RF power investigated (see Fig. 7). Thus, the amount of bounded hydrogen only cannot account for the band gap in nanocrystalline Si films. In addition there are several ambiguities about the high band gap of nanocrystalline Si films because the material contains both phases, amorphous and crystalline and their properties vary with the volume fraction of these phases. The band gap of a-Si:H is between 1.6 and 1.8 eV depending on the process parameters whereas that of c-Si is 1.1 eV. Accordingly, the band gap of nanocrystalline Si should lie between band gap values of a-Si:H and c-Si. On the other hand band gap values obtained in the present study were found greater than 2 eV over the complete range of RF power studied. The high band gap for nanocrystalline Si films prepared by HW-CVD and PE-CVD methods has been reported by various research groups [35, 36]. We think that high band gap of nanocrystalline Si may be due to increase in structural disorder in the films with increase in RF power. It lowers the absorption in the film and shifts the transmission curve towards higher photon energy. This produces higher band gap, which is estimated by extrapolation of absorption curve on the energy axis. Decrease in static refractive index with increase in RF power support this (Fig. 9). The refractive index was estimated by the conventional optical expressions which have been employed by Manifacier et al. [37] and Swanepoel [18]. It has been reported that the refractive index is a measure of the density of the material [38]. Decrease in static refractive index is indicative of a disordered and porous material possibly caused by the increase in Si–H_2 and $(Si–H_2)_n$ complexes in the films with increase in RF power. The higher value of band gap is further strengthened by the observed variation in defect density and Urbach energy (E_U) with RF power. Figure 10 shows the variation of defect density and E_U of films deposited at various RF powers by PE-CVD. As seen from the figure, both defect density and E_U increases with increase in RF power. The E_U also called Urbach tail band width defines the width of the exponential tail of density of states, which extends into the band gap. Usually, it is an indication of structure disorder, where a higher value indicates higher disorder. Increase in E_U and defect density indicates increase in structure disorder in the film with increase in RF power which may be due to increasing number of nc-Si grains and the associated grain boundaries which are known to be normally highly defective [32]. Increase in deposition rate with increase in RF power further support this conjecture (Fig. 2). Generally, the films are more disordered in nature due to the increase in the

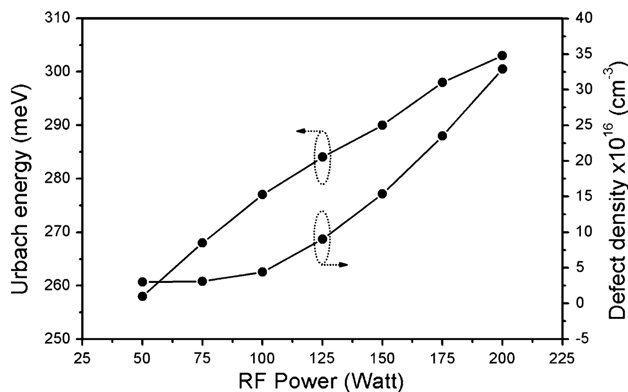

Fig. 10 Variation of defect density and Urbach energy of films deposited at various RF powers by PE-CVD

deposition rate with increase in RF power. In addition, increasing intensity of Si–O–Si stretching mode absorption band $\sim 1060\ cm^{-1}$ [25] in FTIR spectra suggest increasing concentration of O impurity in the film with increasing RF power. The excess oxidation appears to be associated with an increase in the defect density, resulting in disordered structures [39].

3.6 Dark conductivity and activation energy

Figure 11 shows effect of RF power on dark conductivity (σ_{Dark}) and charge carrier activation energy (E_{act}). As seen from the figure, initially the dark conductivity increases with increases in RF power up to 125 W. Then it declines with further increase in RF power. The highest dark conductivity was obtained for the film deposited at RF power 125 W. The high dark conductivity can attributed to crystalline volume fraction of the materials. The Raman spectroscopy analysis supports this. As seen from the Raman spectra (Fig. 4) the highest volume fraction of crystallites has been obtained for the film deposited at RF power of 125 W. The charge carrier activation energy shows reverse trend with respect to dark conductivity. The charge carrier activation energy was found in the range 0.62–0.66 eV over the entire range of RF power studied. These results indicate that the Fermi energy level (E_F) is located near conduction band by defect states in the distorted network at the transition between crystallites and the nearby amorphous matrix [40].

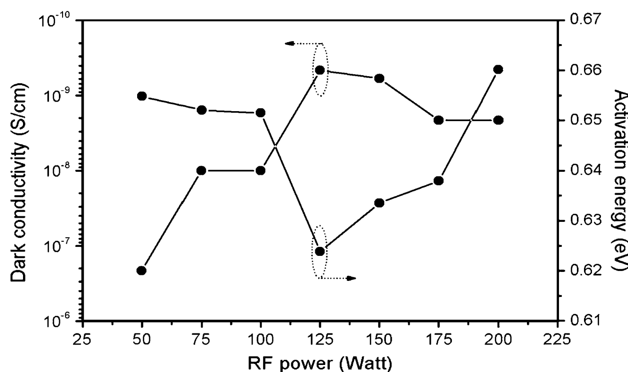

Fig. 11 Effect of RF power on dark conductivity (σ_{Dark}) and charge carrier activation energy (E_{act}) of films deposited at various RF powers by PE-CVD

4 Conclusions

Hydrogenated nanocrystalline silicon (*nc*-Si:H) thin films were prepared by home-made PE-CVD system. We investigated the effect of RF power on the structural, optical and electrical properties of nc-Si:H films by using various characterization techniques. The obtained results exhibited that the deposition rate increases with increase in RF power. Low angle XRD and Raman spectroscopy analysis revealed that the RF power in PE-CVD is a critical process parameter to induce nanocrystallization in Si:H films. The FTIR spectroscopy analysis results indicate that with increase in RF power the predominant hydrogen bonding in films shifts from Si–H to Si–H_2 and (Si–H_2)$_n$ bonded species bonded species. However, the bonded hydrogen content didn't show particular trend with change in RF power. The UV–Visible spectroscopy analysis shows that the band gap values estimated using E_{04} method are found higher than E_{Tauc} values calculated from Tauc's method suggesting increase in band tail width of material with increase in RF power. The defect density and Urbach energy (E_U) also increases with increase in RF power. The highest dark conductivity (and lowest charge carrier activation energy) was obtained for the film deposited at RF power of 125 W indicating that 125 W is optimized RF power of our PE-CVD unit. At this optimized RF power nc-Si:H films with crystallite size $\sim$3.7 nm having good degree of crystallinity ($\sim$86.7 %) and high band gap ($E_{Tauc} \sim$ 2.01 eV and $E_{04} \sim$ 2.58 eV) were obtained with a low hydrogen content (6.2 at.%) at moderately high deposition rate (0.24 nm/s). Further detailed experiments are required to study the effect of other process parameters to optimize the nc-Si:H films before starting n- and p-type doping for solar cells applications.

Acknowledgments The authors are thankful to Department of Science and Technology (DST) and Ministry of New and Renewable Energy (MNRE), Government of India, New Delhi for the financial support. One of the authors S.R.J. is thankful to University Grants Commission, New Delhi for special financial support under UPE program. Mr. Ashok Jadhavar is thankful to collaborative program between Bhabha Atomic Research Center, Mumbai 400 085 and Savitribai Phule Pune University, Pune 411 007 Fellowship and financial assistance.

References

1. H.P. Zhou, D.Y. Wei, S. Xu, S.Q. Xiao, L.X. Xu, S.Y. Huang, Y.N. Guo, W.S. Yan, M. Xu, J. Appl. Phys. **110**, 023517 (2011)
2. G.B. Tong, Z. Aspanut, M.R. Muhamad, S.A. Rahman, Vacuum **86**, 1195 (2012)
3. P. Dutta, S. Paul, D. Galipeau, V. Bommisetty, Thin Solid Films **518**, 6811 (2010)
4. A. Banerjee, F.S. Liu, D. Beglau, S. Tining, G. Pietka, J. Yang, S. Guha, IEEE J. Photovolt. **2**, 104 (2012)
5. J. Yang, B. Yan, S. Guha, Thin Solid Films **487**, 162 (2005)
6. L. Zhang, H.L. Shen, X.F. Jiang, B. Qian, Z.D. Han, H.H. Hou, J. Mater. Sci. Mater. Electron. **24**, 4209 (2013)
7. A.A.D.T. Adikaari, N.K. Mudugamuwa, S.R.P. Silva, Sol. Energy Mater. Sol. Cells **92**, 634 (2008)
8. J.H. Shim, S. Im, Y.J. Kim, N.H. Cho, Thin Solid Films **503**, 55 (2006)
9. B.T. Goh, C.K. Wah, Z. Aspanut, S.A. Rahman, J. Mater. Sci. Mater. Electron. **25**, 286 (2014)
10. S.E. Lee, Y.C. Park, J. Korean Phys. Soc. **65**, 651 (2014)
11. N.A. Bakr, A.M. Funde, V.S. Waman, M.M. Kamble, R.R. Hawaldar, D.P. Amalnerkar, V.G. Sathe, S.W. Gosavi, S.R. Jadkar, J. Phys. Chem. Solids **72**, 685 (2011)
12. H. He, C. Ye, X. Wang, F. Huang, Y. Liua, ECS J. Solid State Sci. Technol. **3**(5), Q74 (2014)
13. S. Peng, D. Wang, F. Yang, Z. Wang, F. Ma, J. Nanomater. Article ID 327596 (2015)
14. M. Brodsky, M. Cardona, J.J. Cuomo, Phys. Rev. B **16**, 3556 (1977)
15. J. Tauc, Mater. Res. Bull. **5**, 721 (1970)
16. T. Kaneko, M. Wakagi, K. Onisawa, T. Minemura, Appl. Phys. Lett. **64**, 1865 (1994)
17. Y. He, C. Yin, G. Cheng, L. Wang, X. Liu, G.Y. Hu, J. Appl. Phys. **75**, 797 (1994)
18. R. Swanepoel, J. Phys. E Sci. Instrum. **16**, 1214 (1983)
19. D. Marquardt, J. Soc. Ind. Appl. Math. **11/2**, 431 (1963)
20. Z. Li, W. Li, Y. Jiang, H. Cai, Y. Gong, J. He, J. Raman Spectrosc. **42**, 415 (2011)
21. G.B. Tong, M.R. Muhamad, S.A. Rahman, Sains Malaysiana **41/8**, 993 (2012)
22. G. Lucovsky, Solar Cells **2**, 431 (1980)
23. S. Halindintwali, D. Knoesen, R. Swanepoel, B. Julies, C. Arendse, T. Muller, C. Theron, A. Gordijn, P. Bronsveld, J.K. Rath, R.E.I. Schropp, Thin Solid Films **515/2**, 8040 (2007)
24. J.C. Knights, G. Lucovsky, R.J. Nemanich, J. Non-Cryst. Solids **32**, 393 (1979)
25. D. Tsu, G. Lucovsky, B. Dadison, Phys. Rev. B **40**, 1795 (1989)
26. A. Jones, W. Ahmed, I. Hassan, C. Rego, H. Sein, M. Amar, M. Jackson, J. Phys.: Condens. Matter **15**, S2969–S2975 (2003)
27. H. Shanks, C. Fang, M. Cardona, F. Demond, S. Kalbitzer, Phys. Status Solidi B **100**, 43 (1980)
28. C.Z. Chen, S.H. Qiu, C.Q. Liu, W.Y. Dan, P. Li, Y.C. Ying, X. Lin, J. Phys. D Appl. Phys. **41**, 195413 (2008)
29. K.X. Lin, X.Y. Lin, Y.P. Yu, H. Wang, J.Y. Chen, J. Appl. Phys. **74**, 4899 (1993)
30. M. Kondo, M. Okada, S. Ohta, L. Guo, A. Matsuda, J. Non-Cryst. Solids **84**, 226 (2000)
31. C. Das, S. Ray, J. Phys. D Appl. Phys. **35**, 2211 (2002)
32. A. Cremona, L. Laguardia, E. Vassallo, G. Ambrosone, U. Coscia, F. Orsini, G. Poletti, J. Appl. Phys. **97**, 023533 (2005)
33. S.B. Amor, M. Atyaoui, R. Bousbih, I. Haddadi, W. Dimassi, H. Ezzaouia, Sol. Energy **108**, 126 (2014)
34. J. Wallinga, W.M. Arnoldbik, A.M. Vredenberg, R.E.I. Schropp, W.F. Van der Weg, J. Phys. Chem. B **102**, 6219 (1998)
35. A. Mahan, R. Biswas, L. Gedvilas, G. Williamson, B. Pan, J. Appl. Phys. **96**, 3818 (2004)
36. P. Gogoi, H. Jha, P. Agarwal, Thin Solid Films **518**, 6818 (2010)
37. J.C. Manifcacier, J. Gasiot, J.P. Fillard, J. Phys. E Sci. Instrum. **9**, 1002 (1976)
38. K.F. Feenstra, Ph. D. thesis, Utrecht University, 47 (1998)
39. G. Lucovsky, R.J. Nemanich, J.C. Knights, Phys. Rev. B **19**, 2064 (1979)
40. P.G. Lecomber, G. Willeke, W.E. Spear, J. Non-Cryst. Solids **59–60/2**, 795 (1983)